Line broadening by hot and dense plasmas*

Nguyen Hoe, J. Grumberg, M. Caby, E. Leboucher, and G. Coulaud

Laboratoire de Spectroscopie Atomique des Plasmas, D. R. P., L. A. N° 71, Université P. et M. Curie, 4, Place Jussieu, 75230 Paris Cedex 05, France

and G. R. E. C. O. Interaction Laser-Matière du Centre National de la Recherche Scientifique, Ecole Polytechnique, 91120 Palaiseau, France

(Received 2 June 1980; revised manuscript received 17 October 1980)

This study is devoted to the broadening of hydrogenic x-ray lines emitted by plasmas produced by laser impact or implosion. In addition to the traditional broadening processes due to high- and low-frequency components of the electric microfield, we have examined the influence of the self-generated magnetic field $\vec{B}$ correlated with the Doppler effect by the motional electric field $\vec{E}_m = \vec{V}_E \times \vec{B}/c$. For the interaction between plasma electrons and radiating ions with high charge number Z_E, fully quantum-mechanical results [Phys. Rev. A **19**, 2421 (1979)] have been used to include all multipole orders of the Coulomb interaction. An analytical treatment of the combined effect of the ion microfield and the self-generated magnetic field shows clearly that the latter is quite important. Its influence consists principally in giving the line profiles a sensitive dependence on polarization and the observation direction $\vec{k}$. In case of the C VI resonance line emitted from a plasma corresponding to the critical density in glass laser experiments and a magnetic field of about 10 MG, the profiles are considerably broader than those deduced from only the particle fields. In addition, the profiles observed parallel to the magnetic field ($\vec{k}//\vec{B}$) may show a central dip which cannot be ignored in a quantitative study of the line absorption properties.

I. INTRODUCTION

With the high-power lasers used in several laboratories, it is now possible to produce hot and extremely dense plasmas. In fact, along the laser-target axis, the plasma electron density increases rapidly up to the solid density $\gtrsim 10^{23}$ cm^{-3} from its critical value of 10^{19} or 10^{21} cm^{-3} according to whether a CO_2 or Nd laser is involved. Simultaneously, the electron temperature decreases from several kilo electron volts in the critical layer to a few hundred electron volts or less in the super-dense layer.

Several recent measurements[1,2] have shown that the study of the Stark profile of x rays of hydrogenic ions with high charge number Z_E provides access to both the electron density and the size of the plasmas obtained by laser implosion. In other respects, due to the crossing of the temperature and density gradients, the resonant absorption, and other mechanisms of lesser importance, the intense self-generated magnetic field and its detrimental effect on the electron transport coefficients have been pointed out in many theoretical works.[3] Hitherto, the experimental determination of this field is essentially based on the Faraday rotation effect on a probe laser beam.[4] Despite the inaccuracy due to the time-dependent aspect and to the uncertainty concerning the plasma geometry, previous measurements show undeniably that magnetic fields are effectively generated and can reach the order of several megagauss.

As far as conventional plasmas with lower electron densities are concerned, it is useful to recall the accuracy and efficiency of the diagnostic based on the impact theory worked out for overlapping lines by Baranger[5] and Griem *et al.*[6] This theory has been generalized for the case of a plasma subject to a magnetic field by Nguyen Hoe *et al.*[7] who considered the competition of Stark and Zeeman effects in connection with the electron collisions. In particular, these authors showed that if the line-profile wings remain practically those of the usual Stark broadening, the central part has a complex structure evolving in a continuous manner between the Paschen-Back effect and the Stark effect in increasing order of the ratio of the ionic microfield E_i to the magnetic field B. Calculation of the $H\alpha$ line shows good agreement with the measurements obtained in a pulsed discharge.[8] Another experimental study was undertaken more recently by Finken[9] who pointed out the possibility of deducing the magnetic field intensity from the absorption properties of a line emitted by a dense plasma.

When the radiating atom or ion is moving fast, a new complication arises from the fact that the optical electron is sensitive to the motional electric field[8] $\vec{E}_m = \vec{V}_E \times \vec{B}/c$ which correlates the Doppler effect with other effects of the magnetic field. The special case of tokamak plasmas, with very high temperature and low electron density, was dealt with by Galushkin,[10] Isler,[11] and Breton *et al.*,[12] who ignored the influence of collisions and electric microfield.

For laser plasmas, characterized by a wide range of temperatures and electron densities, magnetic field influence must be examined in great detail for a quantitative study of line broad-

ening. In effect, in the vicinity of the critical layer where the self-generated magnetic field is intense and the electron density relatively low, the emitted line profile depends on the polarization and observation directions. If the magnetic field is generated in a hot part of the plasma, it is necessary to combine the motional field $\vec{E}_m$ with the ionic microfield $\vec{E}_i$ to study the atomic-level perturbation. When the former cannot be ignored, it may be noted that the correlation existing between radiating particle motion and other broadening mechanisms prevents use of the convolution procedure usually applied to include the Doppler effect in the line profiles.

In the following, we assume that the influence of the plasma electric and magnetic fields is more important than the fine-structure effect and radiative corrections. The specific cases of lines highly influenced by these relativistic effects [proportional to $(Z_E^2/137)^2$, where $\frac{1}{137}$ is the fine-structure constant] will be the subject of a separate study.

Contrary to the special case of the unmagnetized plasmas, the line profile depends on the directions of polarization $\vec{e}$ and observation $\vec{k}$. It can be defined by the following equations:

$$I_{\vec{e},\vec{k}}(\omega,\vec{B}) = \langle I_{\vec{e},\vec{k}}(\omega,\vec{B},\vec{F},\vec{V}_E)\rangle_{\vec{F},\vec{V}_E}, \tag{1}$$

$$I_{\vec{e},\vec{k}}(\omega,\vec{B},\vec{F},\vec{V}_E) = \frac{1}{\pi}\mathrm{Re}\sum_{ijkl}\langle\psi_i|\vec{e}\cdot\vec{r}|\varphi_j\rangle\langle\varphi_l|\vec{e}\cdot\vec{r}|\psi_k\rangle\rho_i \times\left\langle\psi_i\left|\left\langle\varphi_j\left|\left[i\left(\omega-\delta\frac{H^{(n)}(\vec{B},\vec{F},\vec{V}_E)-H^{(n')}(\vec{B},\vec{F},\vec{V}_E)}{\hbar}\right)-\phi^{(nn')}\right]^{-1}\right|\psi_k\right\rangle\right|\varphi_l\right\rangle, \tag{2}$$

where, as in the following, the notation $\langle\ldots\rangle_x\ldots$ means the average over the stochastic variables x... of the plasma. In Eq. (2) we have designated by $\vec{F}$, the resultant electric field; by $\delta = 1+\vec{V}_E\cdot\vec{k}/c$, the factor taking into account the Doppler effect; by ψ_i and φ_j, respectively, the higher and lower state wave functions of the radiative transitions contributing to the line profile; by ρ_i, the diagonal elements of the density matrix; by $H^{(n)}$ and $H^{(n')}$, the Hamiltonians including the quasistatic perturbations and acting, respectively, in the subspaces with unperturbed energy $E_n^0 = -Z_E^2e^2/2a_0n^2$ and $E_{n'}^0 = -Z_E^2e^2/2a_0n'^2$; and by $\phi^{(nn')}$, the dynamic broadening operator expressing essentially the electron contribution.

For Lyman-series lines, starting from fully quantum-mechanical results[13] given by the method of distorted waves, Griem *et al.*[14] have recently suggested the following electron broadening operator:

$$\phi^{(n1)} = \frac{4\pi}{3}\left(\frac{2m}{\pi kT}\right)^{1/2}N_e\left(\frac{\hbar}{m}\right)^2\frac{\vec{r}\cdot\vec{r}}{a_0^2}\left(C_n+\tfrac{1}{2}\int_y^\infty\frac{e^{-x}dx}{x}\right), \tag{3}$$

where $C_2 = 1.5$, $C_3 = 1.0$, $C_4 = 0.75$, ... are strong collision constants and y is the square of the ratio between atomic radius $\langle r\rangle = n^2a_0/Z_E$ and the maximum impact parameter $\rho_{max} = [2kT/m(\omega_p^2+\Delta\omega^2+\Delta E_s^2/\hbar^2)]^{1/2}$. Here, the presence of the plasma frequency $\omega_p = (4\pi N_e e^2/m)^{1/2}$, the frequency separation from the unperturbed line $\Delta\omega = \omega-\omega_0$ and the energy shift due to quasistatic perturbations ΔE_S allows for screening of the electron fields. finite duration of the collisions, and level splittings, respectively. We note that in Eq. (3), inelastic collisions and all multipole orders are included.

II. ENERGY LEVELS AND LINE INTENSITIES UNDER THE COMBINED EFFECT OF ELECTRIC AND MAGNETIC FIELDS

This section is devoted to the treatment of interaction for which the characteristic time is greater than the time of interest $t = \Delta\omega^{-1}$. Firstly, we consider the self-generated magnetic field $\vec{B}$. Recent experiments[4] tend to show that its principal source is the plasma inhomogeneity, characterized by the crossing of electron temperature and electron density gradients in the critical layer. The magnetic field then possesses an axial symmetry around the laser beam. Its intensity can reach several megagauss and its direction is possibly reversed according to reversed density gradient in the off-axis density profile[4].

Secondly, we consider the microfield $\vec{E}_i$, the strength of which is of the same order as that of the normal field $\vec{E}_0 = 2.603e\overline{Z}_i^{1/3}N_e^{2/3}$, where $\overline{Z}_i$ is the average value of perturbing ion charge numbers. The total electric field $\vec{F}$ is the resultant of the microfield $\vec{E}_i$ and the motional field $\vec{E}_m$ that we have already discussed in the introduction:

$$\vec{F} = \vec{E}_i+\vec{E}_m, \quad \vec{E}_m = \vec{V}_E\times\vec{B}/c\,. \tag{4}$$

Assuming that the foregoing fields are intense enough to decouple the spin $\vec{s}$ and the orbital angular momentum $\vec{l}$, the quasistatic interaction potential may be written

$$V_S = e\vec{r}\cdot\vec{F} + \frac{e}{2mc}\vec{l}\cdot\vec{B}, \tag{5}$$

where the term $e\vec{s}\cdot\vec{B}/mc$, having no effect on frequencies and transition probabilities, has been dropped in order to simplify the writing. In the unperturbed energy subspace $E_n^0 = -Z_E^2 e^2/2a_0 n^2$, the potential V_S can be analytically diagonalized by introducing the symmetry O(4) characteristic vectors[15]

$$\vec{j}^{(\pm)} = \tfrac{1}{2}(\vec{l} \pm \vec{g}), \tag{6}$$

where

$$\vec{g} = (-m/2E_n^0)^{1/2}[(1/2m)(\vec{p}\times\vec{l} - \vec{l}\times\vec{p}) - Z_E e^2 \hat{r}]$$

is the Runge-Lenz vector, proportional to the optical electron position vector $\vec{r}$ in accordance with the equation[16]

$$\vec{r} = -(-9/8mE_n^0)^{1/2}\vec{g}, \tag{7}$$

which is valid when matrix elements are taken between states of the same unperturbed negative energy E_n^0. Between two different subspaces with $E_{n'}^0 \neq E_n^0$, the position vector $\vec{r}$ has much more complicated properties and has to be identified with other vectors no longer in SO(4) but in SO(4, 1), which is a dynamical group for the whole set of hydrogenic bound states.

Expressing $\vec{r}$ and $\vec{l}$ in terms of $\vec{j}^{(\pm)}$, the potential (5) then becomes

$$V_S = \omega_L(\vec{u}^{(+)}\cdot\vec{j}^{(+)} + \vec{u}^{(-)}\cdot\vec{j}^{(-)}), \tag{8}$$

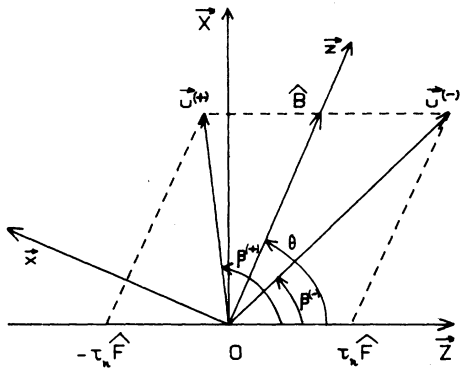

FIG. 1. Geometry of quasistatic interactions $\vec{B}$ and $\vec{F} = \vec{E}_i + \vec{E}_m$. The vector addition $\vec{u}^{(\mp)} = \vec{B}/B \pm \tau_n \vec{F}/F$ allows us to diagonalize analytically the quasistatic interaction potential in accordance with the symmetry properties O(4) of hydrogenic ions.

where

$$\omega_L = eB/2mc,$$
$$\vec{u}^{(\pm)} = \hat{B} \mp \tau_n \hat{F},$$
$$\tau_n = 3na_0 eF/2Z_E\hbar\omega_L.$$

The coefficient τ_n is the ratio of Stark effect to Paschen-Back effect already introduced in our previous papers.[7]

The diagonalization of V_S is straightforward if we remember that vectors $\vec{j}^{(\pm)}$ commute and obey the commutation rules of angular momentum. In particular, with the reference system defined by Fig. 1, eigenvalues and eigenvectors can be expressed

$$\Delta E_S(m^{(+)}, m^{(-)}) = \hbar\omega_L(u^{(+)}m^{(+)} + u^{(-)}m^{(-)}) \tag{9}$$

$$|\psi^{(n)}(m^{(+)}, m^{(-)})\rangle = \sum_{m^{(+)'}, m^{(-)'}} d^{(n-1)/2}_{m^{(+)}m^{(+)'}}(\beta^{(+)}) d^{(n-1)/2}_{m^{(-)}m^{(-)'}}(\beta^{(-)}) \left|\frac{n-1}{2}, m^{(+)'}\right\rangle \left|\frac{n-1}{2}, m^{(-)'}\right\rangle, \tag{10}$$

where

$$j^{(\pm)}\left|\frac{n-1}{2}, m^{(\pm)}\right\rangle = \hbar m^{(\pm)}\left|\frac{n-1}{2}, m^{(\pm)}\right\rangle, \quad -\frac{n-1}{2} \leq m^{(\pm)} \leq \frac{n-1}{2}. \tag{11}$$

As an example, Fig. 2 shows the shift ΔE_S in terms of τ_n and $\theta = (\vec{F}, \vec{B})$ for the first four excited states ($n = 2$). In Eq. (10), the rotation matrix elements allow us to take into account the angular distances $\beta^{(\pm)}$ between vectors $\vec{u}^{(\pm)}$ and the axis $\overrightarrow{OZ} \parallel \vec{F}$. By using the angular momentum addition theorem for: $\vec{l} = \vec{j}^{(+)} + \vec{j}^{(-)}$ we can also express $|\psi^{(n)}(m^{(+)}, m^{(-)})\rangle$ in terms of $|nlm\rangle$ in compliance with

$$|\psi^{(n)}(m^{(+)}, m^{(-)})\rangle = \sum_{lm} |nlm\rangle\langle nlm|\psi^{(n)}(m^{(+)}, m^{(-)})\rangle,$$

$$\langle nlm|\psi^{(n)}(m^{(+)}, m^{(-)})\rangle = (-)^m(2l+1)^{1/2} \sum_{m^{(+)'}} \begin{pmatrix} (n-1)/2 & (n-1)/2 & 1 \\ m^{(+)'} & m-m^{(+)'} & -m \end{pmatrix} d^{(n-1)/2}_{m^{(+)}, m^{(+)'}}(\beta^{(+)}) d^{(n-1)/2}_{m^{(-)}, m-m^{(+)'}}(\beta^{(-)}). \tag{12}$$

These coefficients are given in Table I for the states with $n = 2$.

For the line-profile calculation, we need the matrix elements of dipole components along different polarization directions. Instead of X, Y, and Z, we are more interested in components

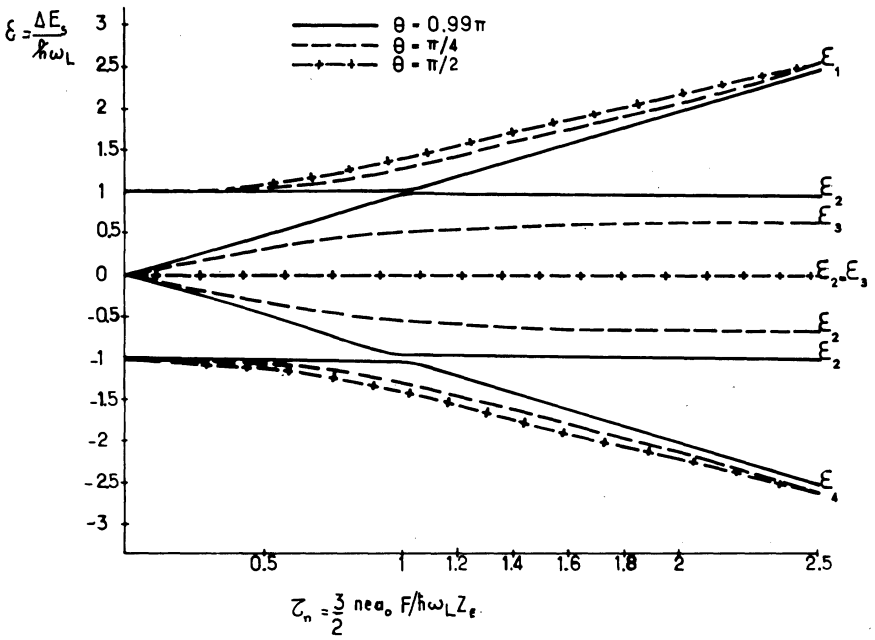

FIG. 2. Shift of levels $n=2$ due to a magnetic field $\vec{B}$ and an electric $\vec{F}[\theta=(\vec{B},\vec{F})]$ acting simultaneously. We observe that the three Zeeman components are obtained by making $\tau_n \to 0$ and that the Stark effect constants are given by the asymptotic slope $\tau_n \to \infty$.

along the magnetic field direction which is, in most cases, a preferential one:

$$\begin{aligned} x &= X\cos\theta - Z\sin\theta\,, \\ y &= Y\,, \\ z &= X\sin\theta + Z\cos\theta\,. \end{aligned} \tag{13}$$

Table II gives the matrix elements of x, y, and z between the ground state $|100\rangle$ and the first four excited states defined by the corresponding energy shifts. Table III gives the intensities and the corresponding values when $\tau_n \to 0$ and $\tau_n \to \infty$ for each polarization direction.

III. LYMAN-α LINE PROFILE CALCULATION

The study of the influence of the quasistatic perturbations is carried out conveniently by introducing the frequencies

$$\begin{aligned} \omega_D &= \frac{\omega_0 \overline{V}_E}{c}\,, \quad \text{where } \overline{V}_E = \left(\frac{2kT_E}{M_E}\right)^{1/2} \\ \omega_S &= \frac{3nea_0E_0}{2Z_E^*\hbar}\,, \quad \text{where } E_0 = 2.603\overline{Z}_i^{1/3}eN_e^{2/3} \\ \omega_m &= \frac{3nea_0B\overline{V}_E}{2Z_E^*\hbar c}\,, \end{aligned} \tag{14}$$

which, respectively, characterize the Doppler effect and the ionic Stark and motional Stark ef-

TABLE I. Energy shift and wave-function coefficients in the $|nlm\rangle$ basis for combined Stark and Zeeman effect.

$\Delta E_S/\hbar\omega_L$ / $n\ l\ m$	$\frac{1}{2}(u^{(+)}+u^{(-)})$	$\frac{1}{2}(u^{(+)}-u^{(-)})$	$-\frac{1}{2}(u^{(+)}-u^{(-)})$	$-\frac{1}{2}(u^{(+)}+u^{(-)})$
2 1 −1	$\sin\frac{\beta^{(+)}}{2}\sin\frac{\beta^{(-)}}{2}$	$\sin\frac{\beta^{(+)}}{2}\cos\frac{\beta^{(-)}}{2}$	$\cos\frac{\beta^{(+)}}{2}\sin\frac{\beta^{(-)}}{2}$	$\cos\frac{\beta^{(+)}}{2}\cos\frac{\beta^{(-)}}{2}$
2 1 0	$\frac{1}{2^{1/2}}\sin\frac{\beta^{(+)}+\beta^{(-)}}{2}$	$\frac{1}{2^{1/2}}\cos\frac{\beta^{(+)}+\beta^{(-)}}{2}$	$\frac{1}{2^{1/2}}\cos\frac{\beta^{(+)}+\beta^{(-)}}{2}$	$-\frac{1}{2^{1/2}}\sin\frac{\beta^{(+)}+\beta^{(-)}}{2}$
2 1 1	$\cos\frac{\beta^{(+)}}{2}\cos\frac{\beta^{(-)}}{2}$	$-\cos\frac{\beta^{(+)}}{2}\sin\frac{\beta^{(-)}}{2}$	$-\sin\frac{\beta^{(+)}}{2}\cos\frac{\beta^{(-)}}{2}$	$\sin\frac{\beta^{(+)}}{2}\sin\frac{\beta^{(-)}}{2}$
2 0 0	$-\frac{1}{2^{1/2}}\sin\frac{\beta^{(+)}-\beta^{(-)}}{2}$	$\frac{1}{2^{1/2}}\cos\frac{\beta^{(+)}-\beta^{(-)}}{2}$	$-\frac{1}{2^{1/2}}\cos\frac{\beta^{(+)}-\beta^{(-)}}{2}$	$-\frac{1}{2^{1/2}}\sin\frac{\beta^{(+)}-\beta^{(-)}}{2}$

TABLE II. Matrix elements of the dipole components between the ground state and the first four excited states ($n=2$). Here we have $\alpha_1=\beta^{(+)}-\theta$ and $\alpha_2=\theta-\beta^{(-)}$, θ being the angle between $\vec{B}$ and $\overrightarrow{OZ}\parallel\vec{F}$.

Polarization \ $\Delta E_S/\hbar\omega_L$	$\frac{1}{2}(u^{(+)}+u^{(-)})$	$\frac{1}{2}(u^{(+)}-u^{(-)})$	$-\frac{1}{2}(u^{(+)}-u^{(-)})$	$-\frac{1}{2}(u^{(+)}+u^{(-)})$
$\frac{x}{2^7 3^{-5}}$	$-\cos\frac{\alpha_1-\alpha_2}{2}$	$\sin\frac{\alpha_1-\alpha_2}{2}$	$\sin\frac{\alpha_1-\alpha_2}{2}$	$\cos\frac{\alpha_1-\alpha_2}{2}$
$\frac{y}{2^7 5^{-5} i}$	$-\cos\frac{\alpha_1+\alpha_2}{2}$	$-\sin\frac{\alpha_1+\alpha_2}{2}$	$\sin\frac{\alpha_1+\alpha_2}{2}$	$-\cos\frac{\alpha_1+\alpha_2}{2}$
$\frac{z}{2^7 3^{-5}}$	$\sin\frac{\alpha_1-\alpha_2}{2}$	$\cos\frac{\alpha_1-\alpha_2}{2}$	$\cos\frac{\alpha_1-\alpha_2}{2}$	$-\sin\frac{\alpha_1-\alpha_2}{2}$

fects. Later, we shall make use of the ratios of these effects to the Zeeman effect, in accordance with the expressions

$$\tau_n^{(0)}=\frac{\omega_S}{\omega_L}=7.369\frac{3n\bar{Z}_i^{1/3}}{2Z_E}\frac{[10^{-20}N_e\ (\mathrm{cm}^{-3})]^{2/3}}{10^{-6}B\ (\mathrm{gauss})}, \quad (15)$$

$$\mu_n=\frac{\omega_m}{\omega_L}=5.422\frac{3n}{2Z_E}\left(\frac{10^{-2}mT_E\ (\mathrm{eV})}{M_E}\right)^{1/2}. \quad (16)$$

Equation (15) must not be confused with the ratio τ_n introduced in Eq. (8) to take account simultaneously the ion microfield $\vec{E}_i=\beta\vec{E}_0$ and the motional electric field $\vec{E}_m$.

For the Lyman-series lines, the profile is then completely defined by the eigenstates of the quasistatic Hamiltonian V_S, Eq. (8), and the diagonal matrix elements $\phi(n,l)$ of the electron broadening operator, Eq. (3), where we recall that[7]

$$\langle nlm|\vec{r}\cdot\vec{r}|nl'm'\rangle=\left(\frac{3na_0}{2Z_E}\right)^2[n^2-(l^2+l+1)]\delta_{ll'}\delta_{mm'}.$$

In the following, we specialize for the Lyα line case, which is of twofold interest. From a theoretical standpoint, on the one hand, this line is sensitive to electron collisions as well as quasistatic and ion-dynamical perturbations. It is possible to stress one of the effects to the detriment of the others by varying plasma parameters B, N_e, T_e, and T_E within a quite realistic region.

Concerning plasma diagnostic, on the other hand, comparison between theory and experiment for the line absorption properties allows us to deduce the plasma geometry[1] or magnetic field[9]. When averaging over polarization direction $\vec{e}$ [perpendicular to the observation direction $\vec{k}(\varphi_0,\theta_0)$] and over the azimuthal angle φ_S of the microfield

TABLE III. Intensities relative to the three polarization directions. The radiative transition corresponding to symmetrical level shifts and intensities are not given in this table. The upper and lower values appearing between accolades correspond, respectively, to the boundary cases $\tau_n\to 0$ (pure Paschen-Back effect) and $\tau_n\to\infty$ (pure Stark effect).

Intensity \ $\Delta E_S/\hbar\omega_L$	$\frac{1}{2}(u^{(+)}+u^{(-)}),\left\{\begin{matrix}1+\frac{\tau_n^2\sin^2\theta}{2}\\ \tau_n\left(1+\frac{\sin^2\theta}{2\tau_n^2}\right)\end{matrix}\right\}$	$\frac{1}{2}(u^{(+)}-u^{(-)}),\left\{\begin{matrix}-\tau_n\cos\theta\\ \cos\theta\end{matrix}\right\}$
$\frac{I_x}{(2^7 3^{-5})^2}$	$\frac{1}{2}\left(1+\frac{1-\tau_n^2\cos 2\theta}{u^{(+)}u^{(-)}}\right),\left\{\begin{matrix}1\\ \sin^2\theta\end{matrix}\right\}$	$\frac{1}{2}\left(1-\frac{1-\tau_n^2\cos 2\theta}{u^{(+)}u^{(-)}}\right),\left\{\begin{matrix}0\\ \cos^2\theta\end{matrix}\right\}$
$\frac{I_y}{(2^7 3^{-5})^2}$	$\frac{1}{2}\left(1+\frac{1-\tau_n^2}{u^{(+)}u^{(-)}}\right),\left\{\begin{matrix}1\\ 0\end{matrix}\right\}$	$\frac{1}{2}\left(1-\frac{1-\tau_n^2}{u^{(+)}u^{(-)}}\right),\left\{\begin{matrix}0\\ 1\end{matrix}\right\}$
$\frac{I_z}{(2^7 3^{-5})^2}$	$\frac{1}{2}\left(1-\frac{1-\tau_n^2\cos 2\theta}{u^{(+)}u^{(-)}}\right),\left\{\begin{matrix}0\\ \cos^2\theta\end{matrix}\right\}$	$\frac{1}{2}\left(1+\frac{1-\tau_n^2\cos 2\theta}{u^{(+)}u^{(-)}}\right),\left\{\begin{matrix}1\\ \sin^2\theta\end{matrix}\right\}$

with $u^{(+)}u^{(-)}=[(1+\tau_n^2)^2-4\tau_n^2\cos^2\theta]^{1/2}$

$\vec{E}_i(\varphi_S, \theta_S, \beta E_0)$, according to Eqs. (1), (2), (3), and to the matrix elements in Table II, the Lyα profile normalized according to the equation $\int I_{\vec{k}}(\tilde{\omega}, \vec{B}) d\tilde{\omega} = 1$ may be written

$$I_{\vec{k}}(\tilde{\omega}, \vec{B}) = \frac{1}{2\pi} \mathrm{Re} \langle \sin^2\theta_0 J_z + (1+\cos^2\theta_0) J_\parallel \rangle_{\vec{v}_E, \theta_S, \beta}, \tag{17}$$

where

$$v_\parallel = \left(\frac{M_E}{2kT_E}\right)^{1/2} v_{E\parallel}, \quad v_\perp = \left(\frac{M_E}{2kT_E}\right)^{1/2} V_{E\perp}, \quad \tilde{\omega} = \frac{\Delta\omega}{\omega_S}$$

$$z_l = (1/\omega_S)\{i[(\tilde{\omega}\omega_S) - \omega_D(v_\parallel \cos\theta_0 + v_\perp \cos\varphi_{v_E} \sin\theta_0)] + \phi(2, l)\} \quad (l = 0, 1)$$

$$\sigma = 1 + (\mu_n v_\perp / \beta \tau_2^{(0)})^2,$$

$$\Delta = z_0 z_1 \left(z_1^2 + \frac{1}{\tau_2^{(0)2}}\right) + \beta^2 \left(\sigma z_1^2 + \frac{1}{\tau_2^{(0)2}} \cos^2\theta_S\right), \tag{18}$$

$$N_z = z_0 \left(z_1^2 + \frac{1}{\tau_2^{(0)2}}\right) + z_1 \beta^2 (\sigma - \cos^2\theta_S),$$

$$N_\parallel = z_0 z_1^2 + z_1 \beta^2 (\sigma + \cos^2\theta_S)/2,$$

$$\gamma = \left[1 - \left(\frac{2\mu_n \beta v_\perp z_1^2 \sin\theta_S}{\tau_2^{(0)} \Delta}\right)^2\right]^{-1/2},$$

$$J_z = \frac{\gamma N_z}{\Delta} + \frac{1-\gamma}{z_1}, \quad J_\parallel = \frac{\gamma N_\parallel}{\Delta} + \frac{1-\gamma}{2z_1}.$$

Note that the factor σ depending on $v_\perp$ correlates the Doppler effect contained in z_l with the other broadening mechanisms. This correlation effect disappears only in the line wings $[\tilde{\omega}\omega_S \gg \phi(2, l),\ \omega_D,\ \omega_m]$ where the line profile, Eq. (17), can be approximated by the sum of the electron contribution $\phi(2, 1)/\pi\omega_S\tilde{\omega}^2$ and the following quasistatic Stark-Zeeman contribution:

$$I_{\vec{k}}^{(S)}(\tilde{\omega}, \vec{B}) = \frac{\tau_2^{(0)3}}{8} \left[\Theta\left(\tilde{\omega} > \frac{1}{\tau_2^{(0)}}\right) \int_{\beta_0}^{\tilde{\omega}} - \Theta\left(\tilde{\omega} < \frac{1}{\tau_2^{(0)}}\right) \int_{\tilde{\omega}}^{\infty}\right] d\beta$$

$$\times \frac{W(\beta)}{\beta(\beta^2 - \beta_0^2)^{1/2}} \left[(\tilde{\omega}^2 - \beta^2)\left(\tilde{\omega}^2 + \frac{1}{\tau_2^{(0)2}}\right)(1+\cos^2\theta_0) + 2\beta_0^2(\beta^2 - \beta_0^2)\sin^2\theta_0\right] \tag{19}$$

where Θ and $W(\beta)$ are the Heaviside function and microfield distribution function, respectively, and

$$\beta_0 = \tilde{\omega}(1 - 1/\tilde{\omega}^2 \tau_2^{(0)2})^{1/2}.$$

The first integral in Eq. (19) leads directly to the Holtsmark profile $\frac{1}{6} W(\tilde{\omega})$ for frequencies larger than ω_L, i.e., $\tilde{\omega} \gg 1/\tau_2^{(0)}$. The second integral is typically due to the magnetic field which couples the shifted and unshifted Stark components. These two parts of the quasistatic profile are illustrated by the curves marked (3) in Figs. 3 and 4, where we note a strong polarization effect expressed by a sensitive dependence with respect to the observation direction $\vec{k}$.

In the absence of the magnetic field ($B = 0$; $\tau_n^{(0)} \to \infty$; $\sigma, \gamma \to 1$), and considering the equations

$$\langle \sin^2\theta_S \rangle_{\theta_S} = \tfrac{1}{2} \langle 1 + \cos^2\theta_S \rangle_{\theta_S} = \tfrac{2}{3},$$

Eq. (17) becomes

$$I_{\vec{k}}(\tilde{\omega}, 0) = I(\tilde{\omega}) = \frac{1}{3\pi} \mathrm{Re} \left\langle \frac{2}{z_1} + \frac{z_0}{z_0 z_1 + \beta^2} \right\rangle_{\vec{v}_E, \beta}, \tag{20}$$

where the first term is due only to the central component broadened by electron collisions and the second term is due to components displaced by the ion microfield, broadened and correlated with the first one by electron collisions.

For plasmas with low temperature and electron density such that it is possible to ignore the influence of the motional electric field ($\mu_n \to 0$) and ion field ($\mu_n^{(0)} \to 0$) we similarly obtain

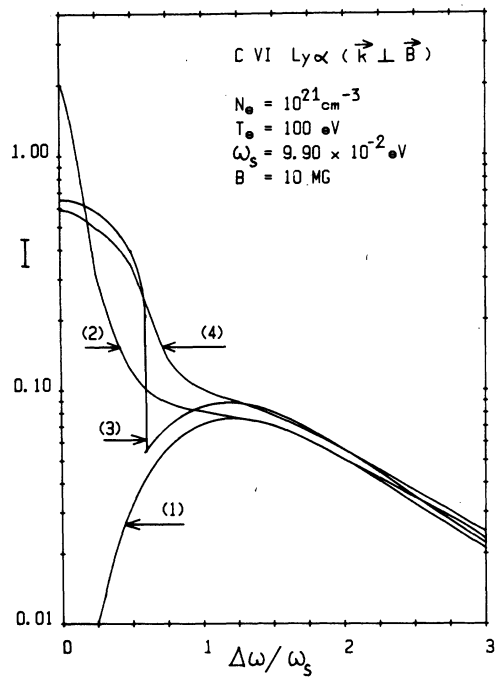

FIG. 3. Line profile observed perpendicular to magnetic field calculated (1) with only the quasistatic ion field effect, (2) with the above and dynamic electron effects, (3) with quasistatic fields $\vec{E}_i$ and $\vec{B}$ combined effects according to Eq. (19), and (4) including $\vec{E}_i$, $\vec{B}$, and electron collisions.

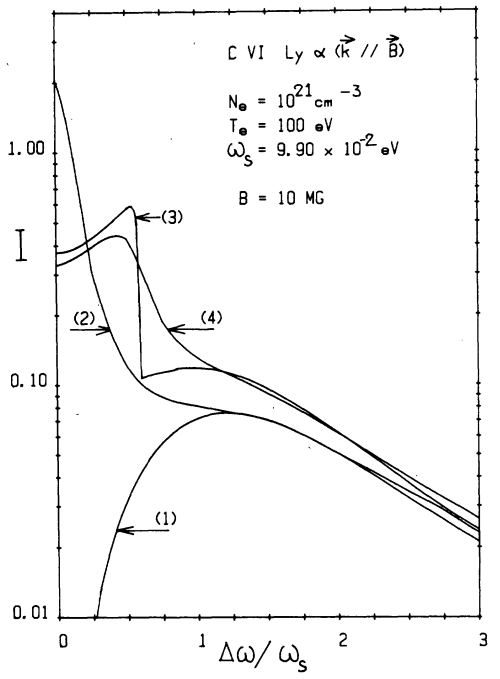

FIG. 4. Same as Fig. 3. except that the observation direction $\vec{k}$ is parallel to the magnetic field.

$$I_{\vec{k}}(\tilde{\omega}, \vec{B}) = \frac{\omega_s}{4\pi} \mathrm{Re} \left\langle (\sin^2\theta_0) \frac{2}{\omega_s z_1} + (1+\cos^2\theta_0) \left(\frac{1}{\omega_s z_1 + i\omega_L} + \frac{1}{\omega_s z_1 - i\omega_L} \right) \right\rangle_{\vec{v}_E}, \tag{21}$$

where we recognize the three components due to the Paschen-Back effect and broadened independently but in the same manner by electron collisions.

Finally, for high temperature and very low electron density tokamak plasmas, ignoring the collisions $[\phi(2,l) \to 0]$ and the Stark effect due to ion microfield ($\tau_2^{(0)} \to 0$), we obtain:

$$I_{\vec{k}}(\tilde{\omega}, \vec{B}) = \frac{\omega_s}{2\omega_L} \left\langle \left(\sin^2\theta_0 + \frac{\mu_n^2 v_\perp^2 (1+\cos^2\theta_0)}{2(1+\mu_n^2 v_\perp^2)} \right) \delta(\Omega) \right.$$

$$\left. + \frac{(2+\mu_n^2 v_\perp^2)(1+\cos^2\theta_0)}{4(1+\mu_n^2 v_\perp^2)} \left[\delta(\Omega + (1+\mu_n^2 v_\perp^2)^{1/2}) + \delta(\Omega - (1+\mu_n^2 v_\perp^2)^{1/2}) \right] \right\rangle_{\vec{v}_E}, \tag{22}$$

where

$$\Omega = (1/\omega_L)\left[\Delta\omega - \omega_D (v_\parallel \cos\theta_0 + v_\perp \cos\varphi_{\vec{v}_E} \sin\theta_0)\right]. \tag{23}$$

For $\mu_n \to 0$, we note that Eq. (22) leads to the three Zeeman components broadened by the Doppler effect. In the general case, via the factor $\mu_n^2 v_\perp^2$, the motional electric field[8,10-12] strongly modulates the line component amplitude and phase. We can see that P states only are involved in the Lyα line formation. While capable of modifying the integrated intensity, the equilibrium conditions peculiar to tokamak plasmas are thus not needed for the expression of the line profile defined in Eq. (22). For lines with higher principal quantum number ($n \geq 3$), we must take these equilibrium conditions into account[11] by introducing appropriate values for the density matrix.

Let us return to the general Eqs. (17) and (18) applicable to laser plasmas where several broadening mechanisms are in competition. The thermal average was obtained numerically by assuming a Maxwellian distribution for the emitting ion velocity $\vec{V}_E$ and by using the microfield distribution

functions $W(\beta)$ calculated by Tighe and Hooper.[17] We have considered the case of a $D-T$ plasma ($\bar{Z}_i = 1$) containing a low percentage of highly ionized ions used as optical probes.

Figures 3 and 4 illustrate the case of the C VI Lyα line subject to the perturbations characteristic of the critical layer. Each perturbation effect can be singled out by comparing suitable curves. We can make the three following remarks.

Line profiles including the magnetic field effect are considerably broader than those deduced from only the particle fields. As already noted about Eq. (19), this comes principally from the contribution of the intense unshifted Stark component which is coupled to the shifted one via the Paschen-Back effect. Also, the difference between curves (3) and (4) shows that the electron broadening is appreciable only on the line wings [via the term $\phi(2,1)/\pi\omega_S\tilde{\omega}^2$] and in the neighborhood of the Larmor frequency (i.e., $\tilde{\omega} = 1/\tau_2^{(0)} = 0.5847$), which is the discontinuity point of quasistatic Stark-Zeeman profiles.

Line profiles are partially polarized as clearly shown by their sensitive dependence with respect to the observation angle $\theta_0 = (\vec{k}, \vec{B})$. The line profile observed parallel to the magnetic field presents a central dip which must be distinguished from the reversal phenomenon due to self-absorption.

In contrast with the unmagnetized plasma case, line profiles are smooth functions of frequency in the central part $|\Delta\omega| \lesssim \omega_L$. Then, only new broadening mechanisms having a characteristic frequency $\omega_c \gtrsim \omega_L$ lead to an important additional effect. Consider, for instance, the Gaussian broadening which originates in field fluctuations caused by electrons in the Debye shielding clouds of ions and improves substantially the comparison between theory[20,21] and experiment[22] on dense and relatively cold plasmas. From Eq. (13) of Ref. 20 and our Eq. (14), the characteristic frequency of ion-dynamical broadening is $\omega_c = (\frac{1}{2}a)^{1/2}\omega_S$, where $a = 2e(\pi N_e^{1/3}/2.603\, kT_e)^{1/2}$ is the electron correlation parameter. With $N_e = 10^{21}$ cm^{-3}, $T_e = 100$ eV, and accordingly $\omega_c \simeq 0.36\ \omega_S$, Figs. 3 and 4 show that corrections at the line center due to ion-dynamical broadening are approximately -15% and + 20% for line profiles, respectively, observed perpendicular and parallel to the assumed magnetic field of 10 MG.

The previous characteristic effects of the magnetic field increase rapidly with the field strength. This is illustrated in Figs. 5 and 6 for C VI Lyα line profiles which were calculated with the same electron density and temperature and different magnetic field strengths. It is interesting to note that in the perpendicular observation case, in contrast with the parallel one, the shifted Zeeman component emerges from the broadened lines only at high magnetic field strength.

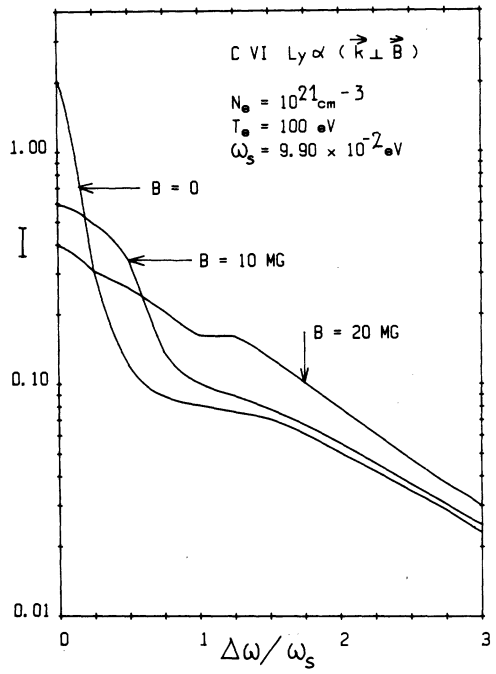

FIG. 5. C VI Lyα line profile calculated with $\vec{k}\perp\vec{B}$ and different magnetic field strengths.

In Fig. 7 we give C VI Lyα line profiles includ-

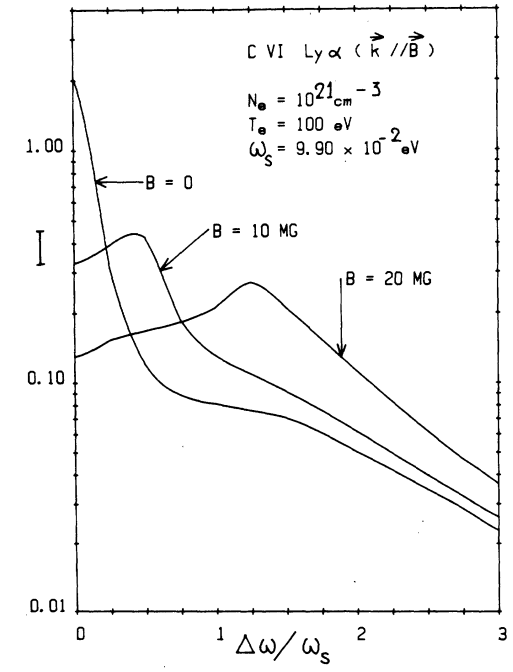

FIG. 6. C VI Lyα line profile calculated with $\vec{k}\parallel\vec{B}$ and different magnetic field strengths.

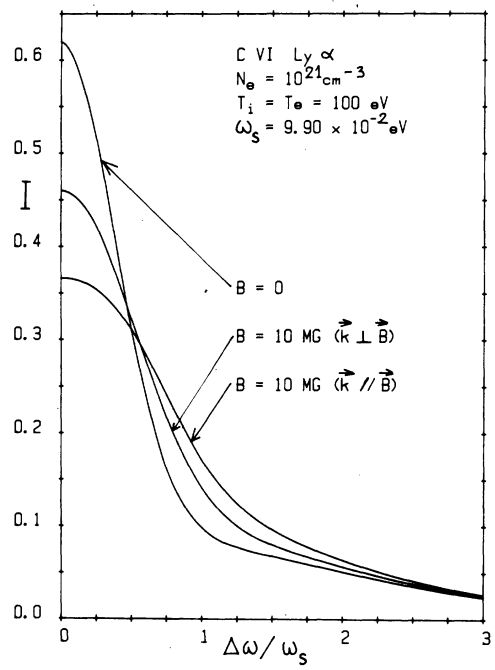

FIG. 7. C VI Lyα line profiles calculated for $B = 0$ and 10 MG and different observation directions. Here, the Doppler and motional Stark effects are included together with magnetic, electron, and ion-broadening effects.

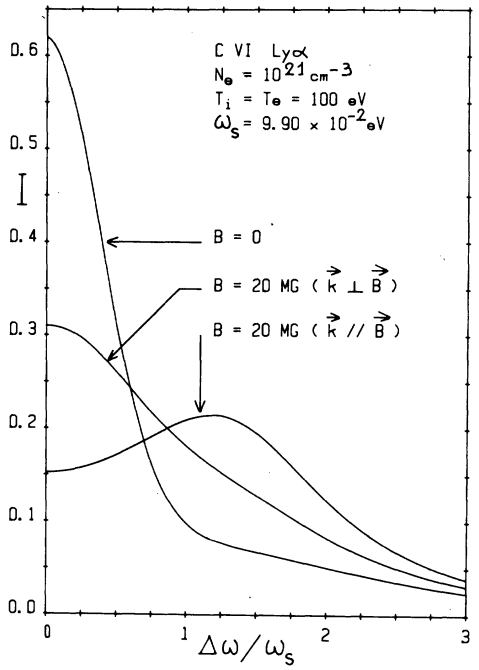

FIG. 8. Same as Fig. 7 except that the magnetic field strength $B = 10$ MG is replaced by $B = 20$ MG. We note the well-marked central dip in the line profile observed parallel to the magnetic field.

ing also the Doppler and motional Stark effects. The numerical calculation shows that the relative effect due to the motional electric field is smaller than 10% throughout the profiles. However, the influence of the magnetic field $B = 10$ MG remains far from negligible. Indeed, perpendicular and parallel observations lead, respectively, to a line width 1.5 and 2 times greater than those observed from a corresponding unmagnetized plasma. We note that the Zeeman structure in the line center is partially masked by the Doppler broadening related to the ion temperature $T_i = 100$ eV. A clearer case is illustrated in Fig. 8 which corresponds to the same ion temperature and to $B = 20$ MG instead of 10 MG and shows clearly a central dip in the line profile observed parallel to the magnetic field.

V. CONCLUSION

We examined the various physical processes likely to contribute to the broadening of highly ionized ion lines in a laser plasma. An analytical method has been proposed in order to include the principal quasistatic perturbations in competition with the Doppler effect: ion microfield, self-generated magnetic field, and motional electric field. The latter, the main cause of line broadening in tokamak plasmas, only makes a marginal contribution (< 10%) in our case. On the other hand, the magnetic field effects must not be ignored in the critical layer radiation study. This consists in polarizing the line profiles and introducing a sensitive dependence with respect to the observation angle $\theta_0 = (\vec{k}, \vec{B})$. For our sample cases, i.e., the C VI resonance line at $N_e = 10^{21}$ cm^{-3} and $B \gtrsim 10$ MG, the profiles are considerably broader than those obtained from an unmagnetized plasma. In addition, the profiles observed parallel to $\vec{B}$ may exhibit a central dip which must be taken into account in a quantitative study of line absorption properties.

These magnetic field effects are particularly important in plasmas that do not have a spherical symmetry, for instance, those obtained from planar targets. They are to be considered together with ion-dynamical effects[19-21] and relativistic effects[18] (for high charge number Z_E) in a realistic comparison between theory and experiment. We note here that the fine-structure splitting of the C VI line is about the same as its Doppler broadening. Inclusion of relativistic effects will therefore diminish the magnetic field effects near the center of the line.

*The results of this study were discussed partially at the National Conference "Collisional Process Influence on Spectral Line Profile." Orléans, 4–5 September 1979 (France). (Invited speaker Nguyen Hoe).

[1]B. Yaakobi, D. Steel, E. Thorsos, A. Hauer, and B. Perry, Phys. Rev. Lett. 39, 1526 (1977); B. Yaakobi, S. Skupsky, R. L. McCrory, C. F. Hooper, H. Deckman, P. Bourke, and J. M. Soures, *ibid.* 44, 1072 (1980); J. M. Auerbach, W. C. Mead, E. M. Campbell, D. L. Matthews, D. S. Bailey, C. W. Hatcher, L. N. Koppel, S. M. Lane, P. H. Y. Lee, K. R. Manes, G. McClellan, D. W. Phillion, R. H. Price, V. C. Rupert, V. W. Slivinsky, and C. D. Swift, *ibid.* 44, 1672 (1980); K. B. Mitchell, D. B. Van Husteyn, G. H. McCall, and P. Lee, *ibid.* 42, 232 (1979); A. Hauer, K. B. Mitchell, D. B. Van Hulsteyn, T. H. Tan, E. J. Linnebur, and M. Mueller, *ibid.* 45, 1495 (1980).

[2]P. Jaegle, A. Carillon, G. Jamelot and C. Wehenkel, J. Phys. (Paris) 40, L551 (1979); A. M. Malvezzi, L. Garifo, E. Jannitti, P. Nicolosi, and G. Tondello, J. Phys. B 12, 1437 (1979).

[3]D. G. Colombant and N. K. Winsor, Phys. Rev. Lett. 38, 697 (1977); C. E. Max, W. M. Manheimer, and J. J. Thomson, Phys. Fluids, 21, 128 (1978); P. Mora and R. Pellat, *ibid.* 22, 2408 (1979).

[4]J. A. Stamper, E. A. McLean, and B. H. Ripin, Phys. Rev. Lett. 40, 1177 (1978); A. Raven, O. Willi, and P. T. Rumsby, *ibid.* 41, 554 (1978).

[5]M. Baranger, Phys. Rev. 112, 855 (1958); in *Atomic and Molecular Processes*, edited by R. Bates (Academic, New York, 1962).

[6]H. R. Griem, A. C. Kolb, and K. Y. Shen, Phys. Rev. 116, 4 (1959); H. R. Griem, *Broadening of Spectral Lines by Plasmas* (Academic, New York, 1974).

[7]Nguyen Hoe, H. W. Drawin, and L. Herman, Z. Naturforsch. 21A, 1515 (1966); J. Quant. Spectrosc. Radiat. Transfer 7, 429 (1967); Nguyen Hoe and H. W. Drawin, Z. Naturforsch. 28A, 789 (1973).

[8]H. W. Drawin, H. Henning, L. Herman, and Nguyen Hoe, J. Quant. Spectrosc. Radiat. Transfer 9, 317 (1969).

[9]K. H. Finken, J. Quant. Spectrosc. Radiat. Transfer. 22, 397 (1979).

[10]Yu. I. Galushkin, Astron. Zh. 47, 375 (1970) [Sov. Astron. 14, 301 (1970)].

[11]R. C. Isler, Phys. Rev. A 14, 1015 (1976).

[12]C. Breton, C. De Michelis, M. Finkenthal, and M. Mattioli, J. Phys. B 13, 1703 (1980).

[13]J. Davis, P. C. Kepple, and M. Blaha, J. Quant. Spectrosc. Radiat. Transfer 16, 1043 (1976).

[14]H. R. Griem, M. Blaha, and P. C. Kepple, Phys. Rev. A 19, 2421 (1979).

[15]J. W. B. Hughes, Proc. Phys. Soc. London, 91, 810 (1967).

[16]G. Flamand, J. Math. Phys. (N.Y.) 7, 1924 (1966).

[17]R. J. Tighe and C. F. Hooper Jr., Phys. Rev. A 14, 1514 (1976); 15, 1773 (1977); 17, 410 (1978).

[18]R. W. Lee, Phys. Lett. 71A, 224 (1979).

[19]D. Voslamber, Phys. Lett. 61A, 27 (1977).

[20]H. R. Griem, Phys. Rev. A 17, 214 (1978).

[21]H. R. Griem, Phys. Rev. A 20, 606 (1979).

[22]K. Grützmacher and B. Wende, Phys. Rev. A 16, 243 (1977).